IOP Publishing and International Atomic Energy Agency Nuclear Fusion

Nucl. Fusion **50** (2010) 025020 (9pp) doi:10.1088/0029-5515/50/2/025020

Advances in global MHD mode stabilization research on NSTX

S.A. Sabbagh[1], J.W. Berkery[1], R.E. Bell[2], J.M. Bialek[1], S.P. Gerhardt[2], J.E. Menard[2], R. Betti[3], D.A. Gates[2], B. Hu[3], O.N. Katsuro-Hopkins[1], B.P. LeBlanc[2], F.M. Levinton[4], J. Manickam[2], K. Tritz[5] and H. Yuh[4]

[1] Department of Applied Physics and Applied Mathematics, Columbia University, New York, NY, USA
[2] Princeton Plasma Physics Laboratory, Princeton University, Princeton, NJ, USA
[3] Laboratory for Laser Energetics, University of Rochester, Rochester, NY, USA
[4] Nova Photonics, Princeton, NJ, USA
[5] Johns Hopkins University, Baltimore, MD, USA

E-mail: sabbagh@pppl.gov

Received 28 August 2009, accepted for publication 8 December 2009
Published 15 January 2010
Online at stacks.iop.org/NF/50/025020

Abstract
Stabilizing modes that limit plasma beta and reduce their deleterious effect on plasma rotation are key goals for the efficient operation of a fusion reactor. Passive stabilization and active control of global kink/ballooning modes and resistive wall modes (RWMs) have been demonstrated on NSTX and research is now advancing towards understanding the stabilization physics and reliably maintaining the high beta plasma for confident extrapolation to ITER and a fusion component test facility based on the spherical torus. Active $n = 1$ control experiments with an expanded sensor set, combined with low levels of $n = 3$ field phased to reduce error fields, reduced resonant field amplification and maintained plasma rotation, exceeded normalized beta = 6 and produced record discharge durations limited by magnet system constraints. Details of the observed RWM dynamics during active control show the mode being converted to a rotating kink that stabilizes or saturates and may lead to tearing modes. Discharges with rotation reduced by $n = 3$ magnetic braking suffer beta collapse at normalized beta = 4.2 approaching the no-wall limit, while normalized beta greater than 5.5 has been reached in these plasmas with $n = 1$ active control, in agreement with the single-mode RWM theory. Advanced state-space control algorithms proposed for RWM control in ITER theoretically yield significant stabilization improvements. Values of relative phase between the measured $n = 1$ mode and the applied correction field that experimentally produce stability/instability agree with RWM control modelling. Experimental mode destabilization occurs over a large range of plasma rotation, challenging the notion of a simple scalar critical rotation speed defining marginal stability. Stability calculations including kinetic modifications to the ideal MHD theory are applied to marginally stable experimental equilibria. Plasma rotation and collisionality variations are examined in the calculations. Intermediate rotation levels are less stable, consistent with experimental observations. Trapped ion resonances play a key role in this result. Recent experiments have demonstrated magnetic braking by non-resonant $n = 2$ fields. The observed rotation damping profile is broader than found for $n = 3$ fields. Increased ion temperature in the region of maximum braking torque increases the observed rate of rotation damping, consistent with the theory of neoclassical toroidal viscosity at low collisionality.

PACS numbers: 52.55.Fa, 52.55.Tn, 52.35.Py, 52.30.-q, 52.30.Cv

(Some figures in this article are in colour only in the electronic version)

1. Introduction

Stabilizing large scale magnetohydrodynamic (MHD) modes that limit plasma beta and reduce their deleterious effect on plasma rotation, ω_ϕ, are key goals for efficient operation of a fusion reactor. Demonstrating steady-state high beta conditions in ITER advanced operational scenarios by passive or active means is a key step towards the high beta operation of DEMO. High beta operation is also important to efficiently achieve neutron fluence goals in a fusion component test facility (CTF) and is required for a demonstration reactor based on the spherical torus (ST) concept. Research on the National

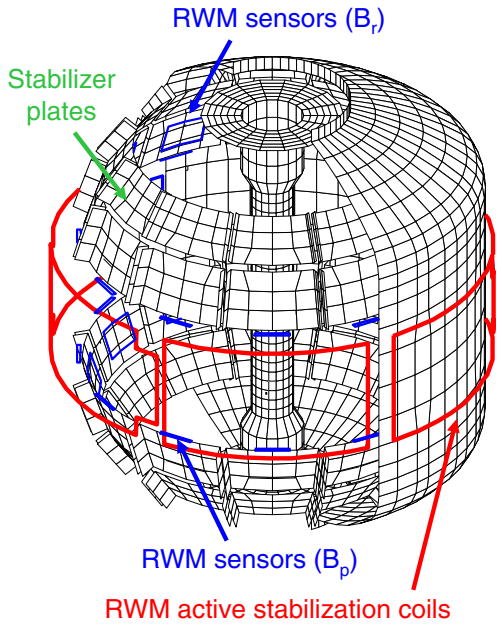

Figure 1. Magnetic stabilization systems on NSTX for finite n modes. Passive stabilization of rotating kink/ballooning modes is provided by the device vacuum vessel and copper stabilizer plates. Active $n = 1$ RWM control is provided by a feedback system utilizing up to 48 sensors, measuring both poloidal and toroidal components of the RWM, and 6 midplane coils that provide the correcting field.

Spherical Torus Experiment (NSTX) has demonstrated both passive stabilization [1] and active control [2] of global kink/ballooning modes and resistive wall modes (RWM) [3–5], accessing high toroidal beta, $\beta_t \equiv 2\mu_0\langle p\rangle/B_0^2 = 39\%$, and normalized beta, $\beta_N \equiv 10^8\langle\beta_t\rangle a B_0/I_p = 7.4$. Here, p is the plasma pressure, B_0 is the vacuum toroidal field at the plasma geometric centre, a is the plasma minor radius at the midplane, I_p is the plasma current and brackets represent volume average. With high beta values reached for many RWM growth times, present experiments and analysis now advance towards understanding and optimizing the performance and reliability of active control to sustain continuous plasma operation at high β_N, understanding global mode stabilization physics and testing present theories of plasma rotation damping due to non-axisymmetric fields (e.g. neoclassical toroidal viscosity (NTV) [6]), which are all important for confident extrapolation to future toroidal magnetic fusion systems.

2. RWM active control

An expanded set of up to 48 resistive wall mode (RWM) sensors was included in recent active $n = 1$ control experiments to determine optimal sensor configurations and relative spatial phasing, and to increase the reliability of maintaining high β_N greater than the ideal MHD no-wall beta limit, $\beta_N^{\text{no-wall}}$. The geometry of this sensor set is shown in figure 1, along with the geometry of the six midplane RWM active control coils and the conducting structure on NSTX (48 copper stabilizing plates in four off-midplane toroidal rings), used to passively stabilize kink/ballooning modes. The vacuum vessel, which also contributes to passive stabilization, is also shown. When

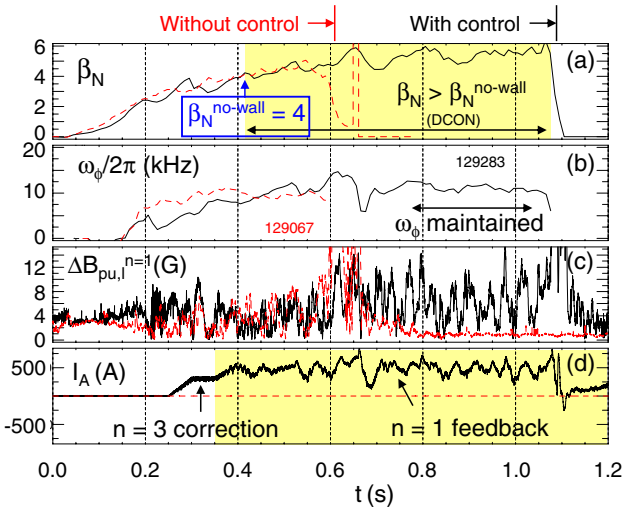

Figure 2. High β_N discharge using $n = 1$ active mode control with B_p sensor arrays above/below the plasma midplane and $n = 3$ dc EFC (solid line) versus a discharge without active control (dashed line) that is terminated by an RWM instability. Frames show the evolution of (*a*) β_N, with the shaded region indicating the period when $\beta_N > \beta_N^{\text{no-wall}}$, (*b*) plasma rotation frequency near the $q = 2$ surface, (*c*) $n = 1$ component of the poloidal field produced by RWM activity and (*d*) current in one of the RWM active feedback coils. The shaded region indicates the period when $n = 1$ feedback is activated.

$n = 1$ active control was combined with low levels of $n = 3$ field phased to reduce error fields, resonant field amplification (RFA) [7] by the stable RWM was reduced and ω_ϕ was maintained, producing record discharge durations in NSTX (up to 1.8 s at $I_p = 0.8$ MA) limited by magnet constraints. Without feedback control, high β_N plasmas are more susceptible to RWM instability leading to disruption, even at high levels of ω_ϕ, and to mode locking at reduced rotation. Figure 2 compares a high β_N discharge using $n = 1$ active mode control with RWM B_p sensor arrays above and below the plasma midplane and $n = 3$ dc error field correction (EFC) to a discharge without active control that is terminated by RWM instability at $\beta_N > \beta_N^{\text{no-wall}}$. In the former case, ω_ϕ is maintained, β_N reaches and exceeds $\beta_N^{\text{no-wall}} = 4$ computed by the DCON stability code [8, 9] and remains above this value with β_N reaching 6 ($\beta_N/\beta_N^{\text{no-wall}} = 1.5$). In the latter case, plasma disruption occurs with ω_ϕ above 8 kHz near the safety factor $q = 2$ surface, significantly larger than the critical value for RWM stabilization of 3.8 kHz observed in experiments using $n = 3$ braking for ω_ϕ control. Discharges both with and without reduced rotation can suffer beta collapse at $\beta_N^{\text{no-wall}} = 4.0$–$4.4$, typical for H-mode pressure profiles, while $\beta_N > 5.5$ has been reached at reduced ω_ϕ with $n = 1$ control [2].

Feedback control of $n = 1$ RFA and unstable RWMs was used as a routine tool for the first time in 2008 on NSTX with more than 200 shots taken in over ten experiments. Two quantifiable measures of success are the probability of reaching long pulse duration and the ability to maintain high β_N. This is expressed by averaging values over the period of constant plasma current in the discharge, e.g. $\langle\beta_N\rangle_{\text{pulse}}$. Restricting the database to standard high performance H-mode operation, high β_N discharges without feedback have a greater susceptibility

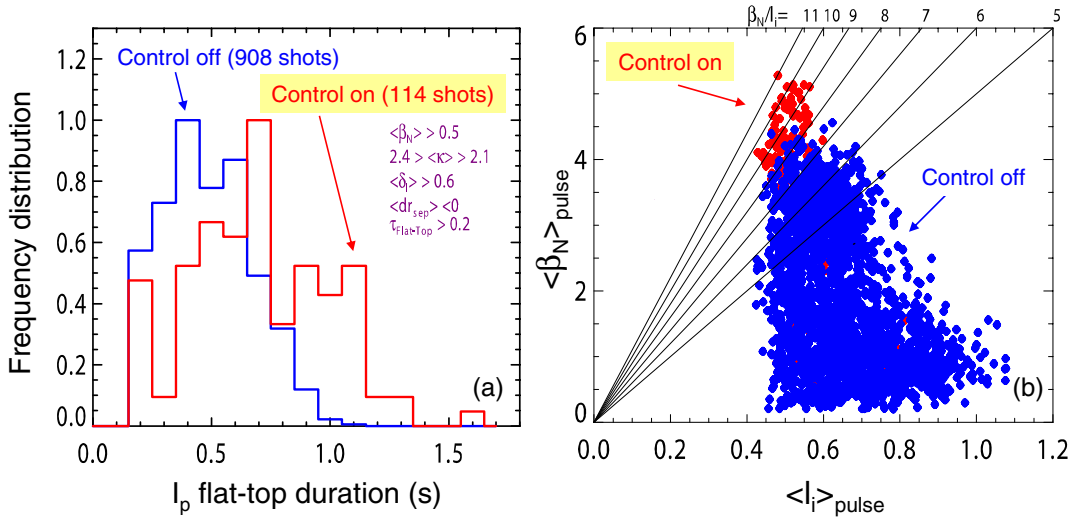

Figure 3. (*a*) Frequency distribution of discharge duration for plasmas with standard high performance H-mode plasma shaping with no $n = 3$ EFC and $n = 1$ feedback control (blue), and with correction and feedback control (red); (*b*) operational stability space showing level of $\langle\beta_N\rangle_{pulse}$ versus $\langle l_i\rangle_{pulse}$ for I_p duration >0.2 s without feedback control (blue), and with control (red).

to RWM-induced disruptions, significantly decreasing the probability of pulse length durations greater than 0.6 s (figure 3(*a*)). With $n = 3$ EFC and $n = 1$ feedback control, I_p flat-top durations of up to 1.6 s were achieved. Figure 3(*b*) shows values of $\langle\beta_N\rangle_{pulse}$ and plasma internal inductance $\langle l_i\rangle_{pulse}$ averaged over the I_p flat-top interval for shots with at least 0.2 s duration (>60 RWM growth times). The highest $\langle\beta_N\rangle_{pulse}$ is maintained with $n = 3$ EFC and $n = 1$ feedback.

Details of $n = 1$ RWM feedback show that control occurs by converting the non-rotating growing RWM into a global kink which either spins up by plasma viscous drag and stabilizes or further leads to energy dissipation by tearing modes. This process provides a link between RWM destabilization and tearing mode onset [10]. The conversion from the RWM to a rotating kink occurs on the eddy current decay time of the wall, $\tau_w \sim 3$–5 ms for $n = 1$ modes. In rare cases, which are the most illustrative, the rotating kink can saturate (figure 4). In this case, RFA observed in the $n = 1$ amplitude of the RWM poloidal field sensors, $\Delta B_p^{n=1}$, precedes the onset of the RWM. As the mode grows to sufficiently high amplitude, increased drag by the toroidal plasma rotation on the mode [1, 6] causes the RWM to unlock and rotate (shown by the $n = 1$ RWM phase, $\Phi_{Bp}^{n=1}$). Without feedback control, this signature leads to further RWM growth and disruption [1]. With feedback, the $n = 1$ control currents (representative current I_A) respond to the mode onset, the RWM unlocks from the wall and accelerates to a frequency in the range of ω_ϕ, precluding the existence of the RWM which damps in $\Delta t \sim \tau_w$. The resulting plasma displacement is identified by ultra-soft x-ray emission (USXR) as a global kink mode (figure 5(*a*)), as it spans a large radial extent in the plasma and shows no phase inversion from the plasma edge to the core (figure 5(*b*)). About 35 ms, or 12 RWM growth times after the saturated kink forms, USXR emission shows a tearing mode displacement form (figure 6). The characteristic phase inversion of the tearing mode displacement is clearly seen across the $q = 2$ surface. The appearance of a tearing mode during the final stage of unstable RWM dynamics has been

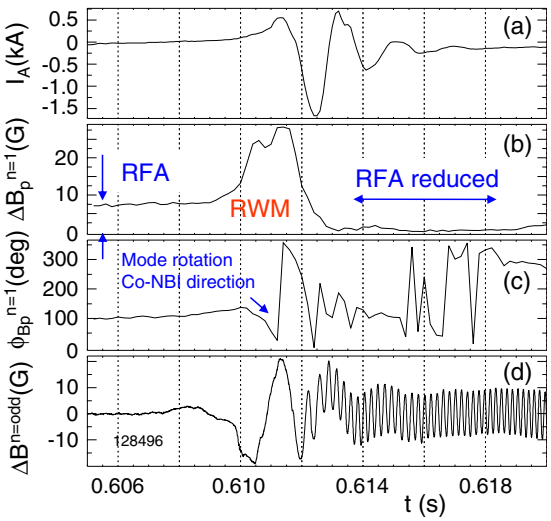

Figure 4. Detail of RWM evolution and feedback current response under active control. Frames show (*a*) current in one of the RWM active feedback coils, (*b*) $n = 1$ component of the poloidal field produced by RWM activity, (*c*) phase of $n = 1$ RWM activity and (*d*) perturbed odd-*n* field amplitude produced by MHD mode activity less than 40 kHz.

recently reported in DIII-D [11]. High frequency fishbone-like activity is also observed at $\beta_N > \beta_N^{no\text{-}wall}$ as recently reported in JT-60U [12], but is not a requirement for RWM destabilization in these plasmas.

Specific $n = 1$ control experiments were run to examine the effect of control system response on RWM control in ITER-relevant low rotation plasmas. As shown in figure 7, control system response was slowed by applying a 75 ms smoothing filter to the requested control field currents (defined as slow feedback or dynamic error field correction (DEFC)) to preclude response to RWM with typical growth times of 3–5 ms. With the smoothing filter applied, mode growth led to disruption at $\beta_N > \beta_N^{no\text{-}wall}$ as ω_ϕ was lowered, showing that slow DEFC alone is insufficient for stabilization at low ω_ϕ. With no filter,

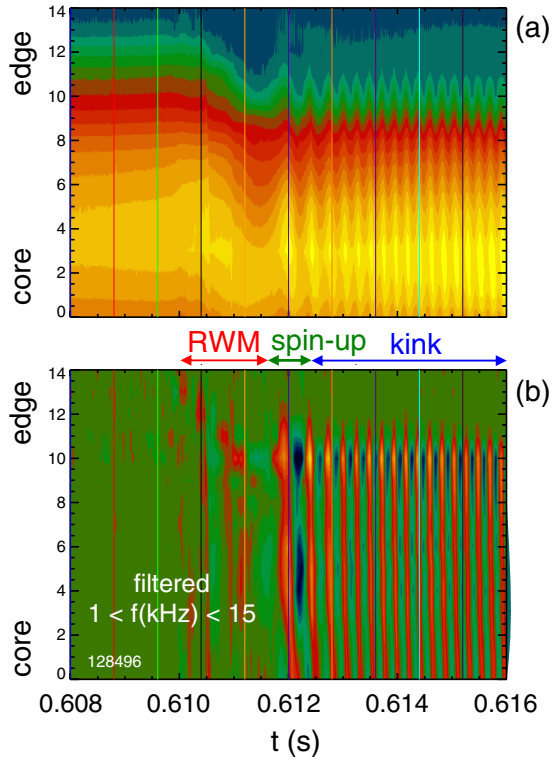

Figure 5. USXR measurement of mode activity during $n = 1$ feedback control: (a) chord integrated signals spanning from the plasma core to edge show RWM onset, unlock and spin-up transition to global kink, (b) filtered USXR signals showing activity in the range 1–15 kHz.

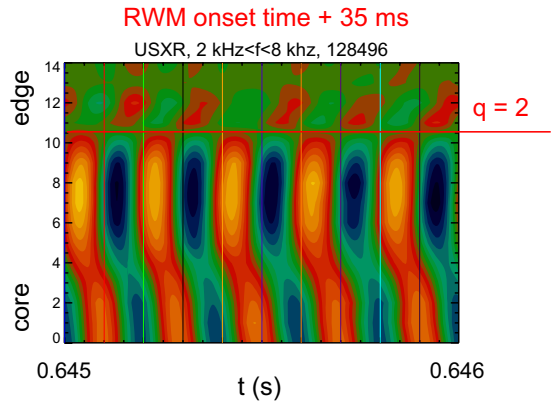

Figure 6. USXR measurements showing the onset of a tearing mode 35 ms (approximately 12 RWM growth times) after RWM onset and conversion to a saturated kink mode, indicated by radial phase inversion of signals across the $q = 2$ surface.

low plasma rotation with ω_ϕ near or below DIII-D balanced NBI levels [13], was produced at high $\beta_N = 5.3$.

Experimental active control performance at reduced plasma rotation was reproduced by the three-dimensional VALEN code [14] with an upgraded system model using the actual off-midplane sensor positions (as shown in figure 1) and applied control field compensation analogous to that used in the experimental feedback system. Discharges with ω_ϕ reduced by $n = 3$ magnetic braking suffer beta collapse at $\beta_N = 4.2$ while approaching the $n = 1$ ideal MHD beta

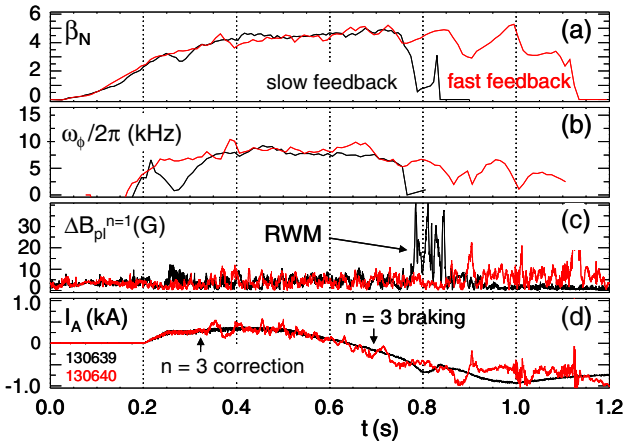

Figure 7. Effect of control system response on $n = 1$ RWM feedback control. Traces in red have no filtering of the control field currents(fast feedback), while traces in red have a 75 ms smoothing filter applied to the control field currents (slow feedback or dynamic EFC). Shown are the evolution of (a) plasma normalized beta, (b) plasma rotation frequency near the $q = 2$ surface, (c) $n = 1$ component of the poloidal field produced by RWM activity and (d) current in one of the RWM active feedback coils.

limit, $\beta_N^{\text{no-wall}}$, as computed by DCON using kinetic plasma reconstructions that include internal magnetic field pitch angle data from a motional Stark effect diagnostic. In contrast, $\beta_N > 5.5$ has been reached in these plasmas with $n = 1$ active control on. This agrees with the single-mode RWM theory computed by the VALEN code using proportional gain, as shown in figure 8(a). Advanced state-space control algorithms proposed for RWM control in ITER [15] theoretically show significant improvements in stabilized β_N up to 6.7 in NSTX. The relative phase, $\Delta\phi_f$, between the measured $n = 1$ mode and the applied correction field theoretically determines if the mode is stabilized or is driven unstable [2]. Values of $\Delta\phi_f$ experimentally producing stability/instability agree with the VALEN theoretical model (figure 8(b)). An analogous model was used to compute the theoretical RWM feedback control performance of ITER advanced scenario 4 equilibria, using the proposed internal coil set and a simple proportional gain control algorithm. An increase in β_N of 50% over $\beta_N^{\text{no-wall}}$ is shown when active control is used (figure 9).

3. RWM passive stabilization physics

Passive stabilization of the RWM by plasma rotation was postulated in early theoretical RWM papers [3, 16–21]; however, a comprehensive physics model that unifies experimental RWM stabilization by rotation remains elusive. RWM passive stabilization has been investigated on NSTX, with results summarized in [22]. A simple scalar threshold describing the critical plasma rotation frequency, Ω_{crit}, or disruption due to loss of torque balance by resonant fields [23] do not describe RWM marginal stability in NSTX which is more profound and shown to be at least related to the plasma rotation profile [22]. The present experiments also use non-resonant magnetic braking techniques in which the applied torque scales linearly with the plasma rotation [24] and does not produce bifurcation of the rotational state. Recent experiments

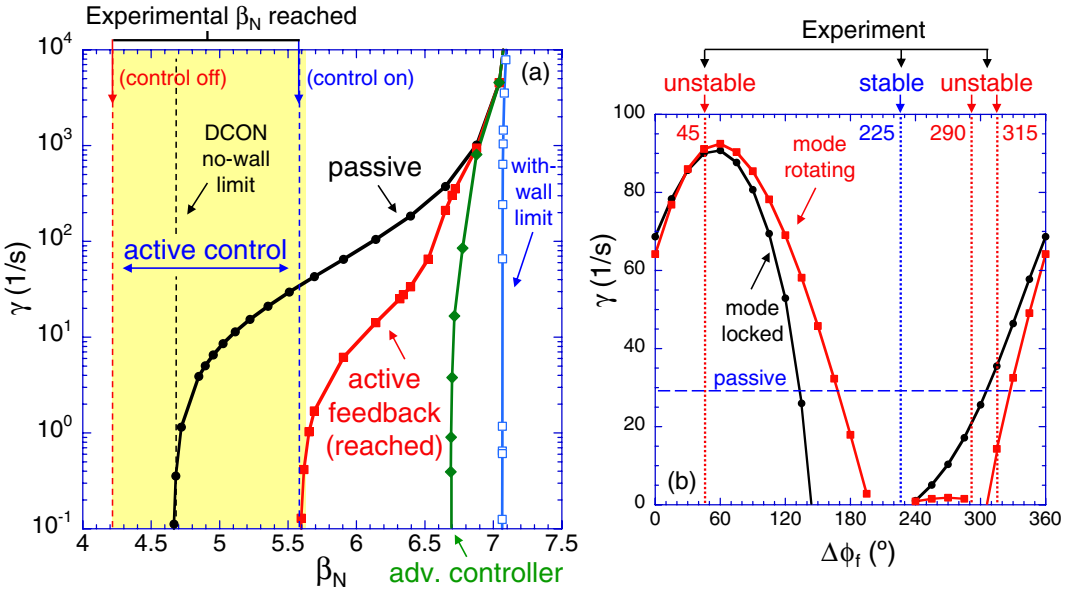

Figure 8. (*a*) Experimental β_N reached with $n = 1$ active control with ω_ϕ reduced by $n = 3$ magnetic braking (shaded region) compared with theoretical feedback control performance using proportional gain. The computed feedback improvement expected from an advanced state-space controller is shown by the labelled dispersion curve. (*b*) Experimental feedback stability versus feedback phase compared with theory. The two curves indicate theoretical results for modes allowed to rotate or forced to remain stationary (locked).

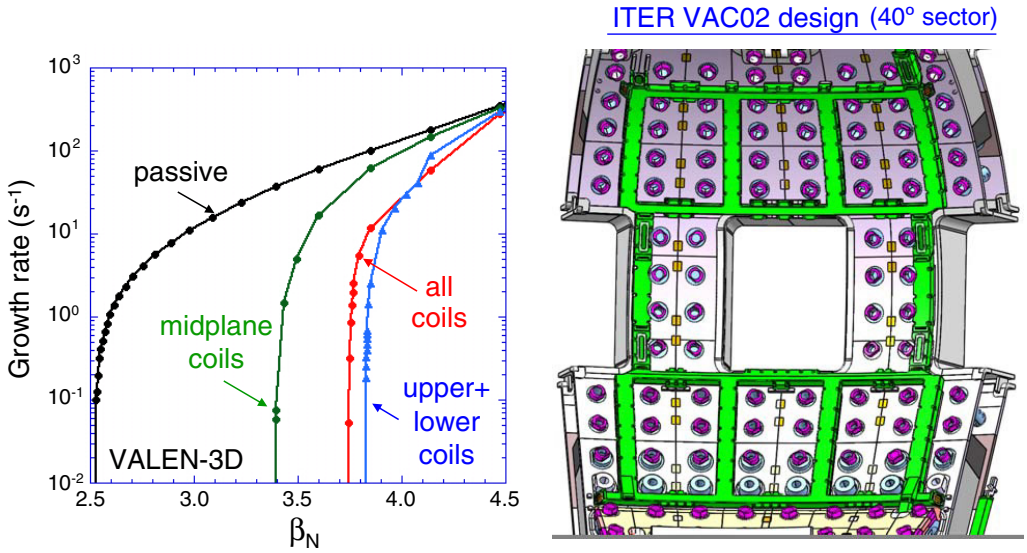

Figure 9. $n = 1$ RWM control performance of present ITER design: (*a*) dispersion curves for passive stabilization and active control using the proposed internal coil set, (*b*) illustration of the proposed internal coil set, showing midplane and off-midplane coil elements.

continue to show this greater complexity. The unstable plasma shown in figure 2 becomes unstable at relatively high $\omega_\phi > 8$ kHz near $q = 2$, while plasmas with ω_ϕ lowered by $n = 3$ non-resonant magnetic braking reach marginal stability at $\omega_\phi = 3.8$ kHz [2]. More recently, $n = 3$ magnetic braking [24] has produced marginally stable plasmas that have $\omega_\phi = 0$ at the $q = 2$ surface. A more comprehensive stability model by Hu and Betti including kinetic modifications to the ideal MHD theory [25] has been used to evaluate the stability of NSTX plasmas with initial success. Modifications to ideal stability by kinetic effects are computed with the MISK code, including the effect of trapped and circulating ions, trapped electrons and Alfven damping [26]. The kinetic components of the perturbed pressure lead to a potential energy functional δW_K. The modified RWM growth rate normalized to τ_w is $\gamma\tau_w = -(\delta W_\infty + \delta W_K)/(\delta W_b + \delta W_K)$, where δW_∞ is δW computed with no stabilizing conducting structure and δW_b is computed with a model of the experimental stabilizing conducting structure. The technique uses a perturbative approach in that the computed marginal RWM eigenfunction is unchanged by kinetic effects, and continuum damping near rational surfaces is computed analytically [26]. The calculation involves integration over energy of a frequency resonance term (equation (5) of [26]). For the trapped ion component,

$$\delta W_K \propto \int \left[\frac{\omega_{*N} + (\hat{\varepsilon} - 3/2)\omega_{*T} + \omega_E - \omega - i\gamma}{\langle\omega_D\rangle + l\omega_b - i\nu_{eff} + \omega_E - \omega - i\gamma} \right] \hat{\varepsilon}^{\frac{5}{2}} e^{-\hat{\varepsilon}} d\hat{\varepsilon}, \quad (1)$$

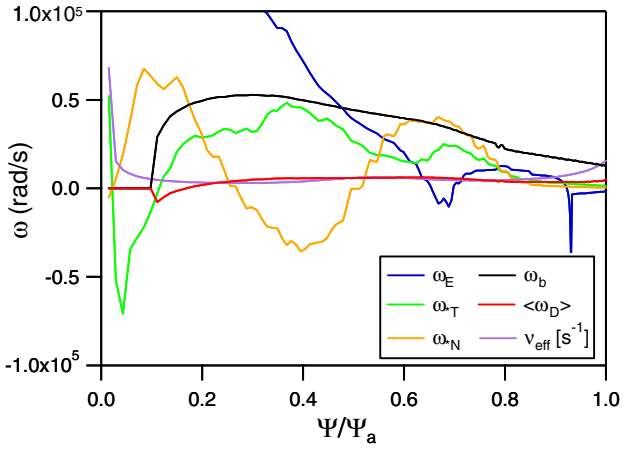

Figure 10. Frequency profiles for kinetic stabilization of RWM marginally stable plasma 121083 at 0.475 s. The collision frequency profile shown is for thermal ions, bounce and diamagnetic frequency profiles are for thermal ions and zero pitch angle.

where the mode frequency is ω and $\hat{\varepsilon}$ is the particle energy normalized to the ion temperature. The other six frequencies are compared, as profiles of poloidal flux Ψ, for an RWM marginally stable plasma in figure 10 where $\omega_{*\mathrm{N}}$ and $\omega_{*\mathrm{T}}$ are the density and temperature gradient components of the ion diamagnetic frequency, ω_{E} is the $E \times B$ frequency, $\langle\omega_{\mathrm{D}}\rangle$ is the bounce-averaged precession drift frequency, ω_{b} is the bounce frequency and ν_{eff} is the effective collision frequency. Plasma toroidal rotation enters through ion force balance $\omega_{\mathrm{E}} = \omega_\phi - \omega_{*\mathrm{N}} - \omega_{*\mathrm{T}}$. The precession drift and bounce resonances in equation (1) allow a more complex dependence of stability on the rotation profile. In the plasma shown in figure 10, $n = 3$ braking produces a peaked ω_ϕ profile, with sufficiently small $|\omega_\phi| < (\omega_{*\mathrm{N}} + \omega_{*\mathrm{T}})$ allowing increased δW_{K} by stabilizing resonance with the trapped ion precession drift in the outer portion of the plasma (roughly $q > 2$). Variation of ω_ϕ from an experimental RWM marginally stable equilibrium reconstruction shows reduced stability at intermediate and low plasma rotation, rather than a simple, single critical rotation threshold. This is shown by varying the experimental rotation profile $\omega_\phi^{\mathrm{exp}}$ and computing the normalized growth rate $\gamma\tau_{\mathrm{w}}$ for these variations. The rotation profile is varied self-similarly from 0.2 to 2 times the experimental profile (figure 11(*a*)). A stability diagram is produced in which contours of constant $\gamma\tau_{\mathrm{w}}$ are shown on a plot of $\mathrm{Im}(\delta W_{\mathrm{K}})$ versus $\mathrm{Re}(\delta W_{\mathrm{K}})$ (figure 11(*b*)). The region of $\gamma\tau_{\mathrm{w}} > 0$ which is theoretically unstable to the RWM is highlighted. Stability decreases as plasma rotation decreases from $\omega_\phi/\omega_\phi^{\mathrm{exp}} = 2.0$ to the value 1.0, which represents the measured experimental profile. This point is experimentally observed to be on the verge of instability and is computed to be close to marginal ($\gamma\tau_{\mathrm{w}} > -0.1$). As ω_ϕ is reduced further, the plasma becomes more stable between $1.0 < \omega_\phi/\omega_\phi^{\mathrm{exp}} < 0.6$. For low rotation ($<0.4\omega_\phi^{\mathrm{exp}}$), the plasma is predicted to be unstable. This is consistent with the general NSTX experimental observation that very low global rotation at $\beta_{\mathrm{N}} > \beta_{\mathrm{N}}^{\mathrm{no\text{-}wall}}$ is typically unattainable without active $n = 1$ control. The region of reduced stability at intermediate levels of rotation is due to a weakening of the stabilizing ion precession drift resonance as plasma rotation is increased from lower levels and the strengthening of the stabilizing bounce resonances at higher levels of plasma rotation.

Further physical insight is attained by examining the components of δW_{K} as rotation is varied. In figure 12 the real and imaginary parts of δW_{K} are broken into the trapped ion, trapped electron, circulating ion and Alfven layer contributions. For $\omega_\phi/\omega_\phi^{\mathrm{exp}}$ from 0.2 to 0.6, stability increases as the real and imaginary trapped ion components increase. From 0.6 to 0.8, the real part increases while the imaginary part decreases, leading to the turn in figure 11 back towards instability. Finally for $\omega_\phi > \omega_\phi^{\mathrm{exp}}$, the trapped ion contributions are nearly constant, but the increase in the circulating ion component leads to increased stability.

Variation of plasma collisionality, ν, from the experimental equilibrium alters the dependence of stability on rotation. Figure 13 shows analogous trajectories to figure 11, but with electron and ion temperatures halved/doubled while the densities are doubled/halved, producing collisionalities increased/decreased by a factor of 5.7 while maintaining constant pressure. Increased ν simplifies the dependence of stability on ω_ϕ, making the trajectory appear more like it has a single critical rotation profile for stability. This might be expected, as higher ν decreases the relative importance of the kinetic resonances. Lower ν produces the opposite effect. As ω_ϕ is decreased, there is a broader reversal of $\gamma\tau_{\mathrm{w}}$ from decreasing to increasing stability, marginal stability occurs at higher plasma rotation than in the actual experiment, and the trajectory shows stability at low ω_ϕ.

4. Plasma rotation alteration by even parity non-resonant fields and T_{i} dependence

Physics understanding of non-axisymmetric field-induced plasma viscosity is important to ITER, especially if magnetic ELM mitigation techniques will be used, and in CTF if ω_ϕ profile alteration is desired for global mode control. Braking torque due to odd parity applied fields has been observed in NSTX and quantitatively compared with the NTV theory [6, 24]. Recent experiments also demonstrate non-resonant braking by an $n = 2$ field configuration generated by the midplane non-axisymmetric coils shown in figure 1. The applied field spectrum has a significant $n = 4$ component (66% of the $n = 2$ amplitude) as well as $n = 8$ and 10 components (each 15% of the $n = 2$ amplitude). The observed rotation damping profile is broader than for $n = 3$ fields (figure 14), which is theoretically expected due to the broader field spectrum and reduced radial falloff of the $n = 2$ field.

A significant aspect of the NTV theory for ITER and a CTF is the strong increase in NTV torque that occurs as the ion collisionality drops below the trapped particle bounce frequency, $\nu_{*\mathrm{i}} < 1$. In this ion collisionality regime, the non-ambipolar flux that leads to NTV is decreasingly perturbed by collisions, which increases the NTV torque, causing a strong dependence on ion temperature, $\tau_{\mathrm{NTV}} \sim \delta B^2 \varepsilon^{1.5} p_{\mathrm{i}}/\nu_{\mathrm{i}} \sim T_{\mathrm{i}}^{5/2}$ [24], where δB is the magnetic field perturbation magnitude, ε is the inverse aspect ratio of the magnetic surface, p_{i} and T_{i} are the ion pressure and temperature, respectively. Recent experiments show that increased T_{i} increases the plasma rotation damping rate during non-resonant magnetic braking. The experiments utilized lithium evaporation to pre-condition

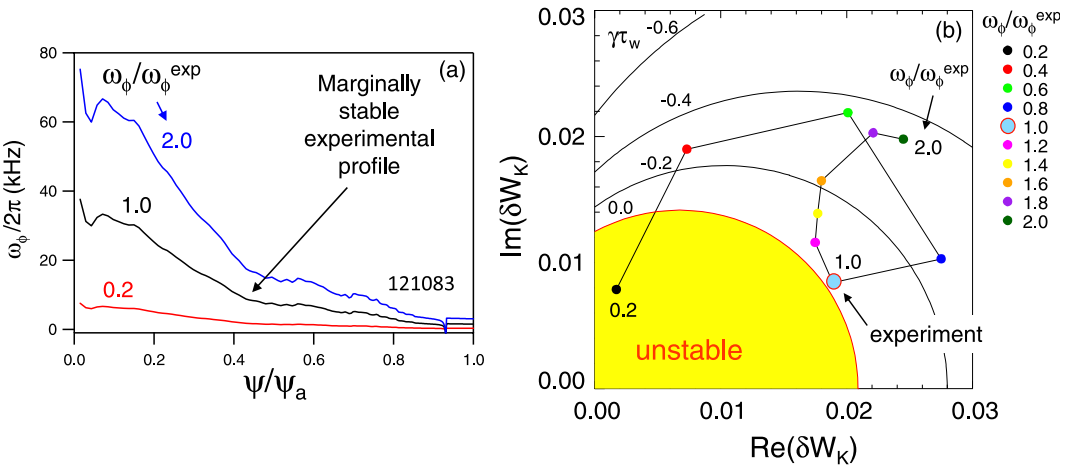

Figure 11. Effect of plasma rotation on $n = 1$ RWM stability for plasma 121083 at 0.475 s. (*a*) shows the marginally stable experimental profile and self-similar variations from it. (*b*) illustrates the theoretical stability variation as the rotation is varied.

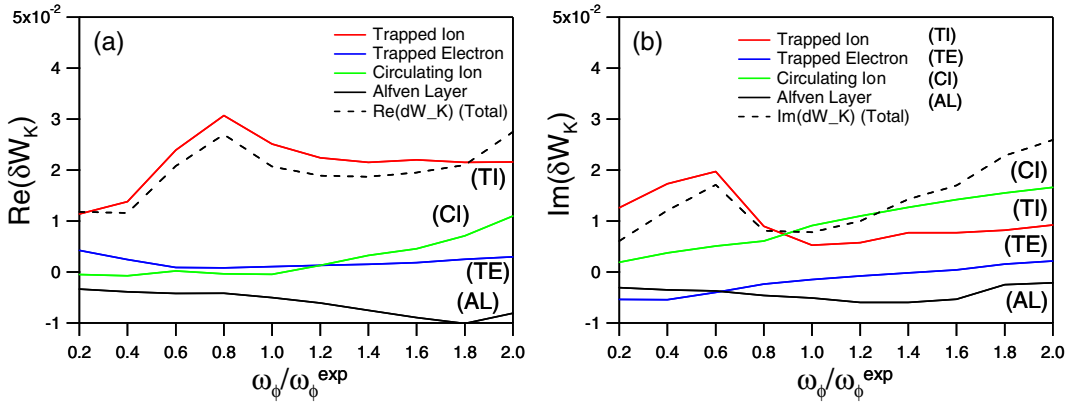

Figure 12. Components of δW_K for plasma 121083 at 0.475 s versus the scaled rotation profile.

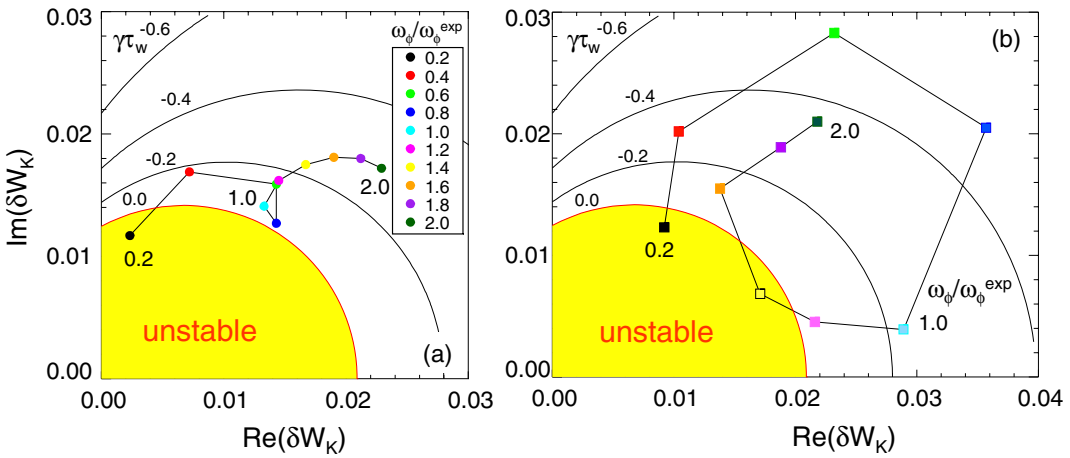

Figure 13. Effect of plasma collisionality on $n = 1$ RWM stability for plasma 121083 at 0.475 s. Solid circles/dashed line indicates ω_ϕ variation at increased v, while open squares/solid line show the ω_ϕ variation at decreased v.

portions of the divertor and plasma facing component carbon tiles [27] to generate a significant increase in T_i in the region of peak $n = 2$ magnetic braking. Figure 15 compares two plasmas with equal magnitude of applied $n = 2$ braking currents, and with/without lithium wall preparation. The plasma with Li wall preparation shows higher initial T_i (shown in the region of maximum change in ω_ϕ, major radial position $R = 1.37$ m) at the start of the magnetic braking pulse, with a ratio of T_i between the two shots of $T_i^{(Li)}/T_i^{(noLi)} = 1.324$. Figure 16 shows the rotation damping profiles for these discharges along with the radial profile of the ratio $T_i^{5/2}$ for these two cases. Plasma rotation reduction is due

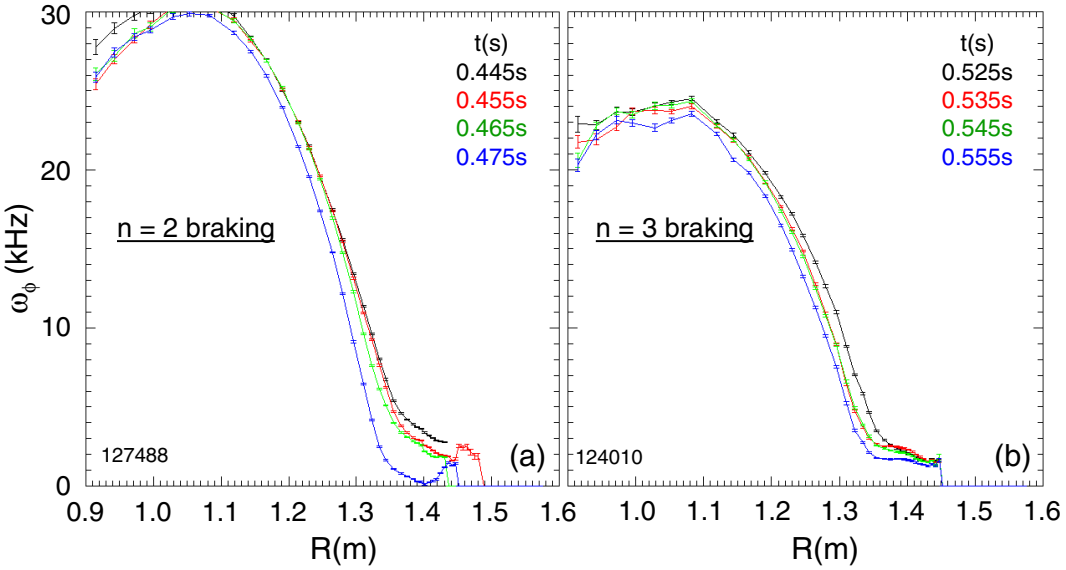

Figure 14. Comparison of non-resonant magnetic braking by (*a*) $n = 2$ field configuration to (*b*) $n = 3$ configuration.

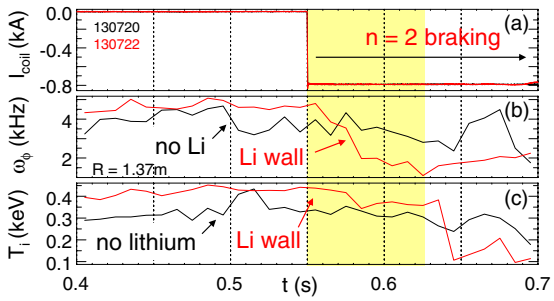

Figure 15. Comparison of $n = 2$ magnetic braking in plasmas with varied ion temperature: (*a*) current in one of the non-axisymmetric midplane coils (maximum current), (*b*) and (*c*) plasma rotation and ion temperature evolution, showing greater plasma deceleration at increased T_i.

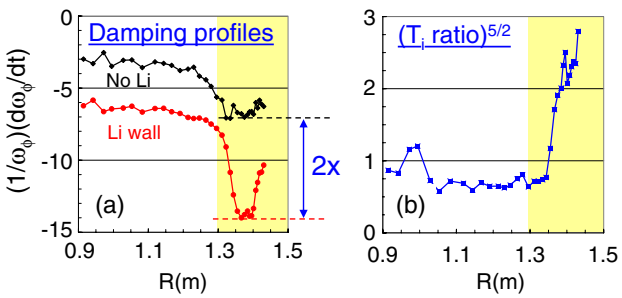

Figure 16. The plasma rotation damping profile (*a*) and ion temperature ratio to the 5/2 power profile (*b*) for plasmas with/without Li wall preparation (130720 and 130722). The region of peak NTV magnetic braking torque is indicated by the shaded region.

to NTV where the applied non-axisymmetric field is largest (indicated by the shaded region in figure 16). The observed factor of two increase in plasma rotation damping rate in the discharge with higher T_i is consistent with the expected increase in the theoretical magnitude of τ_{NTV} based on $T_i^{5/2}$ scaling. Figures 17(*a*) and (*b*) show the plasma rotation profile evolution for these shots. A plasma using Li wall preparation was also run with the $n = 2$ braking current reduced by 25% (~45% less braking torque based on δB^2 scaling) which allowed saturation of the ω_ϕ profile and maintained RWM stability through the braking pulse (figure 17(*c*)).

5. Summary and discussion

With initial passive and active global mode stabilization established on NSTX, research is advancing towards understanding the physics of mode stabilization and to maintaining high beta plasmas with high reliability. RWM instability occurs over a wide range of ω_ϕ, and the combination of $n = 3$ static EFC and $n = 1$ feedback control greatly increases the probability of sustaining high β_N over long pulses, producing record pulse duration in the device, limited by magnet system constraints. Future work will focus on maintaining a high $\langle\beta_N\rangle_{pulse}$ with reduced fluctuation of β_N. RWM dynamics during successful $n = 1$ feedback shows the growing mode convert to a rotating kink which either damps or saturates typically leading to tearing modes. Fast $n = 1$ feedback control response ~O(τ_w) is necessary to avoid high β_N plasma disruption at low ω_ϕ. Experimental active control performance at reduced plasma rotation was reproduced by the VALEN and DCON codes with an upgraded system model. While this model does well to determine the levels of β_N that can be stabilized at reduced plasma rotation, this is only one important consideration for RWM control. The effects of allowing multiple eigenmodes can become important at very high β_N, or with increased core safety factor, and might explain control failures such as mode deformation [2]. This is presently under investigation for NSTX plasmas. In addition, passive RWM stabilization via plasma rotation can experimentally yield significantly higher levels of β_N. A scalar critical rotation threshold for RWM stabilization (for instance, at the $q = 2$ surface) is too restrictive to explain the observed mode destabilization versus plasma rotation [22]. A physics model including kinetic modifications to

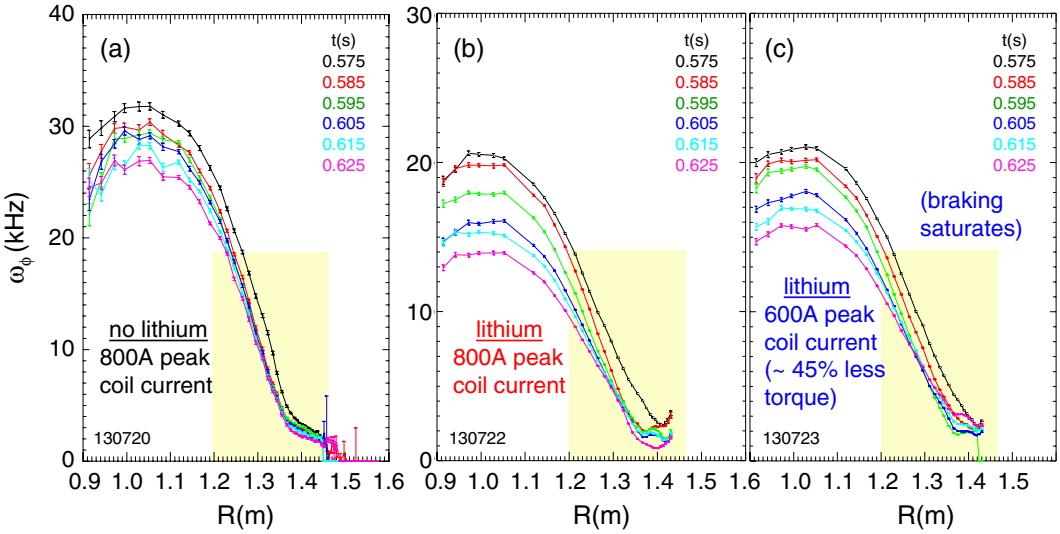

Figure 17. Evolution of ω_ϕ profile in discharges slowed by $n = 2$ magnetic braking. (*a*) and (*b*) pertain to the plasmas without/with Li wall preparation (figures 14-15). (*c*) shows a discharge in which NTV braking saturates at reduced applied field.

ideal stability shows regions of reduced passive stability at intermediate ω_ϕ as well as low ω_ϕ, which are consistent with experimental observations. In such experimental conditions, active RWM control is still be needed to help ensure sustained plasma operation. Plasma collisionality alters the range of ω_ϕ displaying reduced stability, which may unify the physics understanding of RWM stability between present STs and tokamaks. Further investigation is presently underway to understand this NSTX result in connection with tokamak experiments. Plasma rotation alteration has been demonstrated by magnetic braking using non-resonant $n = 2$ fields. The observed rotation damping profile is broader than that found for $n = 3$ fields. Increasing ion temperature in the region of maximum braking torque increases the observed rate of rotation damping, consistent with the dominant scaling of the non-resonant NTV torque $\tau_{NTV} \sim \delta B^2 \varepsilon^{1.5} p_i/\nu_i \sim T_i^{5/2}$ in the NSTX range of collisionality $\nu_{*i} < 1$. Research at lower ν_i is important to determine at what collisionality the $1/\nu_i$ scaling will saturate due to increased radial electric field as the non-ambipolar diffusion causing increases and if τ_{NTV} will eventually decrease as ν_i is further reduced [28].

Acknowledgments

This research was supported by the US Department of Energy under contracts DE-FG02-99ER54524 and DE-AC02-76CH03073.

References

[1] Sabbagh S.A. *et al* 2006 *Nucl. Fusion* **46** 635
[2] Sabbagh S.A. *et al* 2006 *Phys. Rev. Lett.* **97** 045004
[3] Bondeson A. and Ward D.J. 1994 *Phys. Rev. Lett.* **72** 2709
[4] Garofalo A.M. *et al* 1999 *Phys. Rev. Lett.* **82** 3811
[5] Sabbagh S.A. *et al* 2002 *Phys. Plasmas* **9** 2085
[6] Shaing K.C., Hirshman S.P. and Callen J.D. 1986 *Phys. Fluids* **29** 521
[7] Boozer A.H. 2001 *Phys. Rev. Lett.* **86** 5059
[8] Glasser A.H. and Chance M.C. 1997 *Bull. Am. Phys. Soc.* **42** 1848
[9] Newcomb W. 1960 *Ann. Phys.* **10** 232
[10] Sabbagh S.A. *et al* 2004 *Nucl. Fusion* **44** 560
[11] Okabayashi M. *et al* 2009 *Nucl. Fusion* **49** 125003
[12] Matsunaga G. *et al* 2009 *Phys. Rev. Lett.* **103** 045001
[13] Reimerdes H. *et al* 2007 *Phys. Rev. Lett.* **98** 055001
[14] Bialek J.M. *et al* 2001 *Phys. Plasmas* **8** 2170
[15] Katsuro-Hopkins O. *et al* 2007 *Nucl. Fusion* **47** 1157
[16] Ward D.J. and Bondeson A. 1995 *Phys. Plasmas* **2** 1570
[17] Chu M.S. *et al* 1995 *Phys. Plasmas* **2** 2236
[18] Finn J.M. 1995 *Phys. Plasmas* **2** 3782
[19] Betti R. and Friedberg J.P. 1995 *Phys. Rev. Lett.* **74** 2949
[20] Fitzpatrick R. and Aydemir A.Y. 1996 *Nucl. Fusion* **36** 11
[21] Betti R. 1998 *Phys. Plasmas* **5** 3615
[22] Sontag A.C. *et al* 2007 *Nucl. Fusion* **47** 1005
[23] Garofalo A. *et al* 2007 *Nucl. Fusion* **47** 1121
[24] Zhu W. *et al* 2006 *Phys. Rev. Lett.* **96** 225002
[25] Hu B. and Betti R. 2004 *Phys. Rev. Lett.* **93** 105002
[26] Hu B., Betti R. and Manickam J. 2005 *Phys. Plasmas* **12** 057301
[27] Mansfield D.K. *et al* 2009 *J. Nucl. Mater.* **390–391** 764
[28] Shaing K.C., Sabbagh S.A. and Chu M.S. 2009 *Plasma Phys. Control. Fusion* **51** 035004